Circuits, Systems, and Signal Processing
https://doi.org/10.1007/s00034-025-03035-7

Enhancing Time–Frequency Signal Analysis: Integrating Windowing with the Fractional Fourier Transform for Modern Applications

Maykon Silva[1] · **Ricardo Oliveira**[1] · **Flávio Rocha**[1]

Received: 28 December 2024 / Revised: 4 February 2025 / Accepted: 4 February 2025

Abstract

Applications based on sensor data collection, such as respiration and heartbeat monitoring, rely on accurate frequency-domain analysis. Fields such as digital communication and pattern recognition also rely on spectral analysis of sensor-derived data, often leveraging the Fourier Transform (FT) as a key tool. However, FT presents drawbacks, such as spectral leakage, which can be partially mitigated by applying window functions. For critical applications, though, window functions alone may not be enough for optimal performance. Recent studies have explored combining window functions with the Fractional Fourier Transform (FrFT) to enhance results, though success depends on the chosen window function. Among existing options, Nuttall windows offer high attenuation of side lobes, reducing spectral leakage but also presenting a wide main lobe, leading to signal distortion. In this article, we propose a new mathematical model combining Nuttall windows with FrFT. This model provides a closed-form expression, utilizing a parameter to control the main lobe width while maintaining reduced side lobe size, thereby enhancing adaptability for various sensor-based applications. Results show that adjusting the main lobe width using the FrFT expands Nuttall windows' applications, such as in spectral analysis of respiratory signals, where it improves frequency recognition, as well as in Filtered-OFDM to address Out-of-Band Emission, offering an effective solution to one of the major challenges in ensuring spectral efficiency.

✉ Maykon Silva
maykonrenan@discente.ufg.br

Ricardo Oliveira
ricardo_oliveira@discente.ufg.br

Flávio Rocha
flaviogcr@ufg.br

[1] School of Electrical, Mechanical and Computer Engineering, Universidade Federal de Goiás (UFG), Av. Universitária, Goiânia, Goiás 74605-010, Brazil

Published online: 11 March 2025

Keywords FrFT · Nuttall window functions · Sensor applications · Spectral analysis · Spectral leakage

1 Introduction

In recent years, advancements in signal processing have focused on improvements that directly impact digital filter design, data classification, and communication systems, enhancing the accuracy, efficiency, and adaptability of practical applications [2, 7, 11, 12, 16, 22, 28, 33, 35]. For instance, advancements in magnetic resonance imaging through digital filter design [29], disease classification based on medical images [3], and physical layer processing in Beyond 5G (B5G) communication systems [37] are notable examples of recent progress at the frontier of knowledge. These efforts often rely on techniques based on the Fourier Transform (FT) and window functions. While the FT is a powerful and well-established tool in signal processing [18, 21, 31, 32], providing a frequency-domain representation for stationary signals, it has limitations that can be problematic in certain scenarios. For signals with time-varying frequencies (non-stationary signals), the FT's assumptions become invalid, and its application may result in increased spectral leakage and Out-Of-Band Emissions (OOBEs). These issues are typically addressed in the literature through the use of window functions, which are mathematical functions that help reducing spectral leakage by tapering the signal at its boundaries. By smoothing the discontinuities at the edges of the signal, window functions limit the spread of energy across the frequency spectrum, thereby improving the accuracy of the frequency-domain representation. Common examples include the Hamming, Hann, and Blackman windows, each offering a different balance between main lobe width and side lobe attenuation.

Unlike the FT, the Fractional Fourier Transform (FrFT) converts a signal (from time or frequency domain) into an intermediate domain between time and frequency. The FrFT has fractional order, making it a flexible approach, allowing access to any value between time and frequency and finding transformation domains that offer better signal visualization than conventional FT. Most studies in the literature propose algorithms to reduce OOBE using FT-based techniques, which limit applications to scenarios where signals are stationary and their time-domain representations are not critical. For this reason, FrFT is valuable for analyzing non-smooth signals and non-linear systems [19, 39]. In the literature, few contributions combine the FrFT with windowing techniques. In [20], the authors propose a mathematical model to obtain the FrFT of the Dirichlet and Hamming window functions. The FrFT contains an adjustable parameter that controls the main lobe width and, correspondingly, the minimum stopband attenuation of the resulting window function. In [27], a closed-form expression for the FrFT of the generalized triangular window and Welch function is proposed. In [9], a mathematical model is presented to obtain the FrFT of the PC6 window function. According to the authors, for different FrFT order values, the PC6 window function shows variation in different parameters. Thus, changing the order of the FrFT allows the minimum stopband attenuation of the resulting window function to be controlled. In [10, 23], the authors proposed new Finite Impulse Response (FIR) filter models based on window functions combined with the FrFT algorithm. Finally, in [5] the authors propose a new

fractional time-frequency transform, called the windowed Fourier transform (α-WFT), where α is a fractional parameter.

In the cited works where the FrFT is applied, window functions are static, and no scenarios with real-world applications are presented. In this study, we propose a novel algorithm that combines the flexibility of the FrFT with the adaptability of an adjustable window, effectively reducing OOBE and significantly enhancing performance in practical applications, such as contactless human respiratory monitoring and physical layer processing for B5G mobile communications. More specifically, we present in this work the following main contributions that advance the state-of-the-art in signal processing using window functions:

- **A closed-form expression for Nuttall window functions in the FrFT domain.** A mathematical approach that derives a closed-form expression to describe the behavior of Nuttall window functions in the FrFT domain.
- **Application of the proposed approach to healthcare technologies and 5G communication systems.** Using the proposed approach, we obtain reduced spectral leakage in sensor-acquired respiratory signals, improving the recognition of target frequencies and decreasing OOBE and Bit Error Rate (BER) in F-OFDM systems for B5G.

The rest of the article is organized as follows: Sect. 2 presents the background knowlege of window functions and the FrFT; Sect. 3 presents a mathematical approach for analyzing the Nuttall family of windows in the Fourier fractional domain; Sect. 4 evaluates the performance of the proposed approach through spectral analysis and presents the performance of the proposed approach in practical applications involving respiratory signals and wireless networks for B5G use cases; Sect. 5 presents the conclusions and future works.

2 Background

This section presents basic concepts of the key elements used in this work: window functions and FrFT.

2.1 Window Functions and Spectral Parameters

The windowing technique consists of a mathematical function with an amplitude varying smoothly and gradually towards zero at the edges [13]. The frequency response of a window function comprises the main lobe and the side lobes. The main lobe of the window function represents the frequency of interest of the signal, while the side lobes represent the effects of the spectral leakage [28]. However, reducing the side lobes using window function comes with a price, it increases the width of the main lobe, resulting in signal distortion and hardening the frequency domain analysis [8, 13, 28].

The window functions can be either fixed or adjustable. Fixed windows have only one independent parameter (the window length) controlling the main lobe width. Adjustable windows have two or more independent parameters, the window length, as

Table 1 Nuttall window coefficients

Window	a_0	a_1	a_2	a_3
Nuttall 1	0.3750000	0.5000000	0.1250000	0.0126040
Nuttall 2	0.4243801	0.4973406	0.0782793	0.0000000
Nuttall 3	0.3557680	0.4873960	0.1442320	0.0126040
Nuttall 4	0.3635819	0.4891775	0.1365995	0.0106411
Nuttall 5	0.3125000	0.4687500	0.1875000	0.0312500
Nuttall 6	0.3389460	0.4819730	0.1610540	0.0180270

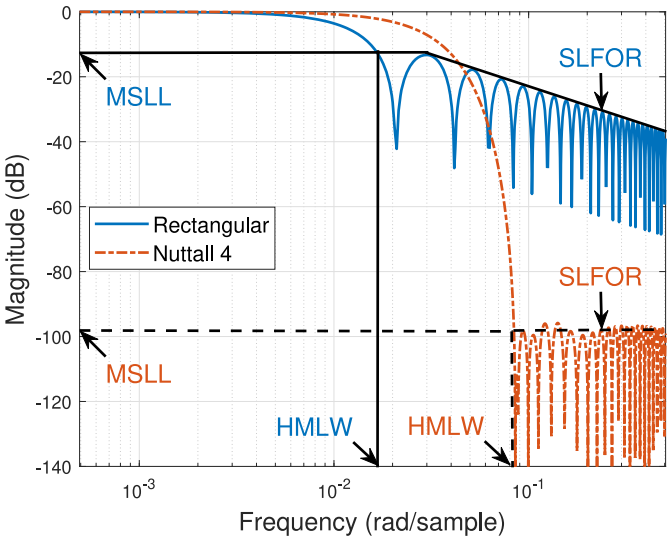

Fig. 1 PSD of the Rectangular and Nuttall 4 windows, along with their parameters

in fixed windows, and one or more additional parameters that control the attenuation of the side lobes [28].

For example, the family of Nuttall window functions are mathematical functions derived from the sum of the cosines of three or four terms [8, 13]. The Nuttall window function in the time domain is given by:

$$w(t) = a_0 + a_1\cos(2\pi t) + a_2\cos(4\pi t) + a_3\cos(6\pi t), \tag{1}$$

where $|t| \leq \frac{1}{2}$. Table 1 presents the coefficients for the Nuttall window functions, where the selection of coefficients is crucial in defining the spectral characteristics of these windows. Further details on Nuttall windows can be found in [25, 28].

Figure 1 illustrates the Power Spectral Density (PSD) for both the Rectangular window and the Nuttall 4 window function. The Nuttall 4 window is particularly interesting for comparison purposes as it exhibits a completely different PSD compared to the reference window (Rectangular). This figure highlights spectral parameters widely

used in spectral analysis to aid the decision-making process for the most appropriate window for each application [8, 13, 28]: Half Main Lobe Width (HMLW) is the frequency at which the main lobe amplitude, when decaying, becomes equal to the largest side lobe amplitude; Maximum Side Lobe Level (MSLL) is the ratio of the peak amplitude of the main lobe to the highest amplitude peak of the side lobe; Side Lobe Fall-Off Rate (SLFOR) is the slope that indicates how quickly the intensity of side lobes decreases as they move away from the main lobe in the frequency domain.

The primary advantage of Nuttall windows lies in their large side lobe attenuation in the frequency domain, achieved after applying the Fourier Transform (FT). This property significantly reduces spectral leakage by concentrating the signal energy in the main lobe, making them superior to other cosine-sum windows like Hamming, Hanning, and Blackman. Such characteristics are particularly beneficial in applications like next-generation mobile communications, where they effectively mitigate OOBE.

However, the low MSLL of Nuttall windows also results in a wide main lobe. This trade-off often necessitates a balance between MSLL and HMLW to suit specific applications. More specifically, a wide main lobe has disadvantages for: (i) healthcare applications, since it increases noise bandwidth and broadens frequency selection, which can hinder spectral analysis and the recognition of distinct frequency patterns, and (ii) wireless communications, since applying windows with this characteristic to baseband signals may lead to interference between adjacent subbands (spectrum subchannels), increasing the BER and ultimately degrading network performance.

2.2 Linear Canonical Transform (LCT) and Fractional Fourier Transform (FrFT)

The Linear Canonical Transform (LCT) is a time-frequency analysis tool that generalizes a wide range of linear transforms. It is defined by a parameterized matrix, which enables a representation of signals across both domains. The LCT encompasses some well-known transforms as special cases, such as the Fourier Transform, the Fresnel Transform, and the FrFT, among others [30, 36]. Mathematically speaking, the LCT of the $x(t)$ signal is defined in function of the parameters μ,ρ,σ,η, as follows:

$$X_{\mu,\rho,\delta,\eta}(u) = \mathcal{F}_{\mu,\rho,\delta,\eta}(x(t)) = \int_{-\infty}^{+\infty} x(t) K_{\mu,\rho,\delta,\eta}(t,u) dt, \tag{2}$$

where $K_{\mu,\rho,\delta,\eta}(t,u)$ is given by:

$$K_{\mu,\rho,\delta,\eta}(t,u) = \begin{cases} \sqrt{\frac{1}{i\rho}} \mathrm{e}^{\left(i\pi\frac{\eta}{\rho}u^2\right)} \int_{-\infty}^{+\infty} \mathrm{e}^{\left(-i2\pi\frac{\eta}{\rho}ut\right)} \mathrm{e}^{\left(i\pi\frac{\mu}{\rho}t^2\right)} x(t)\, dt, & \text{para } \rho \neq 0, \\ \sqrt{\eta}\mathrm{e}^{\left(-i\pi\delta\eta u^2\right)} x(\eta u), & \text{para } \rho \neq 0. \end{cases} \tag{3}$$

The LCT parameters (μ,ρ,σ,η) are written as the LCT parameter matrix A satisfying the determinant constraint $\mu\eta - \rho\sigma = 1$. The values for A determine special cases for the LCT, as presented in Table 2 [36].

Among the special cases for the LCT, we highlight the FrFT, which controls all parameters of the LCT matrix using the so-called rotation angle ($\alpha \in \mathbb{R}$), with great

Table 2 Special cases for the Linear Canonical Transform (LCT)

LCT parameter matrix	Transform
$A = \begin{bmatrix} \mu & \rho \\ \delta & \eta \end{bmatrix} = \begin{bmatrix} 1 & 0 \\ 0 & 1 \end{bmatrix}$	Identity Transform
$A = \begin{bmatrix} \mu & \rho \\ \delta & \eta \end{bmatrix} = \begin{bmatrix} 0 & 1 \\ -1 & 0 \end{bmatrix}$	Fourier Transform
$A = \begin{bmatrix} \mu & \rho \\ \delta & \eta \end{bmatrix} = \begin{bmatrix} \sigma & 0 \\ 0 & \sigma^{-1} \end{bmatrix}$	Scaling Transform
$A = \begin{bmatrix} \mu & \rho \\ \delta & \eta \end{bmatrix} = \begin{bmatrix} 1 & \gamma \\ 0 & 1 \end{bmatrix}$	Fresnel Transform
$A = \begin{bmatrix} \mu & \rho \\ \delta & \eta \end{bmatrix} = \begin{bmatrix} \cos(\alpha) & \sin(\alpha) \\ -\sin(\alpha) & \cos(\alpha) \end{bmatrix}$	Fractional Fourier Transform

time-frequency domain flexibility when compared to the Fourier Transform and other special transform cases. More specifically, the FrFT is an integral transform considered a generalization of the multidimensional FT based on the well-known "rotation" properties (e.g., time-shifting, frequency-shift). The FrFT can be deduced as the FT of the α-th power, which transforms a signal into any intermediate domain between time and frequency [30]. The FrFT is defined as a linear operator as follows:

$$X_\alpha(u) = \mathcal{F}_\alpha(x(t)) = \int_{-\infty}^{+\infty} x(t) K_\alpha(t,u) dt, \tag{4}$$

where $K_\alpha(t,u)$ is given by:

$$K_\alpha(t,u) = \sqrt{\frac{1 - i\cot(\alpha)}{2\pi}} \mathrm{e}^{\left[i\frac{t^2+u^2}{2}\cot(\alpha) - iut\,\mathrm{cosec}(\alpha)\right]}. \tag{5}$$

FrFT is denoted by $\mathcal{F}_\alpha$, where u is the angular frequency, $\alpha = \beta\pi/2$, $\beta \in \mathbb{R}$. For $\beta = 1$, the FrFT reduces to the conventional FT; for integer values of $\beta > 1$, FrFT is equivalent to the successive application of the FT; for $\beta = 0$, it is equivalent to an identity function; for $\beta = -1$, the FrFT is equivalent to the inverse Fourier transform [26].

The FrFT is particularly well-suited to our proposal. Unlike other instances of the LCT, which often have zero elements in their parameter matrix, the FrFT retains all four parameters of the LCT matrix as functions of a single variable, α, the rotation angle. This dependency provides the FrFT with greater flexibility and adaptability while maintaining simplicity, making it an ideal choice for applications requiring smooth transitions between the time and frequency domains.

In this article, we focus on the FrFT because of its ability to fully exploit the parameterization of the LCT matrix, offering advantages that are not present in other LCT special cases. In the next section, we leverage the FrFT flexibility that the α parameter provides to derive a closed-form expression for the Nuttall window functions in the FrFT domain.

3 Closed-Form Expression for Nuttall Window Functions Using FrFT

The FrFT has the unique characteristic of transitioning gradually from the time domain to the frequency domain by adjusting the angular frequency parameter rather than doing so abruptly. By developing a theoretical model that combines the FrFT with Nuttall windows, it became possible to control the width of the main lobe while simultaneously maintaining the reduced size of the side lobes. This control is achieved using the same FrFT parameter-the angular frequency. Consequently, this approach not only broadens the application potential of Nuttall windows but also mitigates their primary drawback compared to Hamming, Hanning, and Blackman windows.

This section presents Proposition 1, a novel closed-form expression for Nuttall window functions in the FrFT domain. This closed-form expression has the advantage of offering a direct analysis for window functions based on the sum of cosine in the Fourier fractional domain, providing control of the spectral parameters introduced in Sect. 2: HMLW, MSLL and SLFOR.

Proposition 1 *Let α be the rotation angle, with $\alpha = \beta\pi/2$. Let u be the angular frequency. A closed-form expression in the FrFT domain capable of controling the main lobe width of the Nuttall window functions depends on the α and u parameters, as follows:*

$$
\begin{aligned}
W_\alpha(u) = {} & \frac{a_0}{2}\sqrt{\frac{1-i\cot(\alpha)}{i\cot(\alpha)}}\, e^{\frac{u^2}{2}\left(i\cot(\alpha)+\frac{\operatorname{cosec}(\alpha)^2}{i\cot(\alpha)}\right)} \\
& \times\left\{\operatorname{erfi}\left(\frac{\sqrt{i/2\cot(\alpha)}}{2}-\frac{iu\operatorname{cosec}(\alpha)}{2\sqrt{i/2\cot(\alpha)}}\right)\right. \\
& \left.-\operatorname{erfi}\left(-\frac{\sqrt{i/2\cot(\alpha)}}{2}-\frac{iu\operatorname{cosec}(\alpha)}{2\sqrt{i/2\cot(\alpha)}}\right)\right\} \\
& +\frac{a_1}{4}\sqrt{\frac{1-i\cot(\alpha)}{i\cot(\alpha)}}\, e^{\left(i\frac{u^2}{2}\cot(\alpha)-\frac{(i2\pi-iu\operatorname{cosec}(\alpha))^2}{2i\cot(\alpha)}\right)} \\
& \times\left\{\operatorname{erfi}\left(\frac{\sqrt{i/2\cot(\alpha)}}{2}+\frac{i2\pi-iu\operatorname{cosec}(\alpha)}{2\sqrt{i/2\cot(\alpha)}}\right)\right. \\
& \left.-\operatorname{erfi}\left(-\frac{\sqrt{i/2\cot(\alpha)}}{2}+\frac{i2\pi-iu\operatorname{cosec}(\alpha)}{2\sqrt{i/2\cot(\alpha)}}\right)\right\} \\
& +\frac{a_1}{4}\sqrt{\frac{1-i\cot(\alpha)}{i\cot(\alpha)}}\, e^{\left(i\frac{u^2}{2}\cot(\alpha)-\frac{(-i2\pi-iu\operatorname{cosec}(\alpha))^2}{2i\cot(\alpha)}\right)} \\
& \times\left\{\operatorname{erfi}\left(\frac{\sqrt{i/2\cot(\alpha)}}{2}-\frac{i2\pi+iu\operatorname{cosec}(\alpha)}{2\sqrt{i/2\cot(\alpha)}}\right)\right. \\
& \left.-\operatorname{erfi}\left(-\frac{\sqrt{i/2\cot(\alpha)}}{2}-\frac{i2\pi+iu\operatorname{cosec}(\alpha)}{2\sqrt{i/2\cot(\alpha)}}\right)\right\} \\
& +\frac{a_2}{4}\sqrt{\frac{1-i\cot(\alpha)}{i\cot(\alpha)}}\, e^{\left(i\frac{u^2}{2}\cot(\alpha)-\frac{(i4\pi-iu\operatorname{cosec}(\alpha))^2}{2i\cot(\alpha)}\right)} \\
& \times\left\{\operatorname{erfi}\left(\frac{\sqrt{i/2\cot(\alpha)}}{2}+\frac{i4\pi-iu\operatorname{cosec}(\alpha)}{2\sqrt{i/2\cot(\alpha)}}\right)\right.
\end{aligned}
$$

$$
\begin{aligned}
&- \operatorname{erfi}\left(-\frac{\sqrt{i/2\cot(\alpha)}}{2} + \frac{i4\pi - iu\operatorname{cosec}(\alpha)}{2\sqrt{i/2\cot(\alpha)}}\right)\Bigg\} \\
&+\frac{a_2}{4}\sqrt{\frac{1-i\cot(\alpha)}{i\cot(\alpha)}}e^{\left(i\frac{u^2}{2}\cot(\alpha)-\frac{(-i4\pi-iu\operatorname{cosec}(\alpha))^2}{2i\cot(\alpha)}\right)} \\
&\times\Bigg\{\operatorname{erfi}\left(\frac{\sqrt{i/2\cot(\alpha)}}{2} - \frac{i4\pi + iu\operatorname{cosec}(\alpha)}{2\sqrt{i/2\cot(\alpha)}}\right) \\
&- \operatorname{erfi}\left(-\frac{\sqrt{i/2\cot(\alpha)}}{2} - \frac{i4\pi + iu\operatorname{cosec}(\alpha)}{2\sqrt{i/2\cot(\alpha)}}\right)\Bigg\} \\
&+\frac{a_3}{4}\sqrt{\frac{1-i\cot(\alpha)}{i\cot(\alpha)}}e^{\left(i\frac{u^2}{2}\cot(\alpha)-\frac{(i6\pi-iu\operatorname{cosec}(\alpha))^2}{2i\cot(\alpha)}\right)} \\
&\times\Bigg\{\operatorname{erfi}\left(\frac{\sqrt{i/2\cot(\alpha)}}{2} + \frac{i6\pi - iu\operatorname{cosec}(\alpha)}{2\sqrt{i/2\cot(\alpha)}}\right) \\
&- \operatorname{erfi}\left(-\frac{\sqrt{i/2\cot(\alpha)}}{2} + \frac{i6\pi - iu\operatorname{cosec}(\alpha)}{2\sqrt{i/2\cot(\alpha)}}\right)\Bigg\} \\
&+\frac{a_3}{4}\sqrt{\frac{1-i\cot(\alpha)}{i\cot(\alpha)}}e^{\left(i\frac{u^2}{2}\cot(\alpha)-\frac{(-i6\pi-iu\operatorname{cosec}(\alpha))^2}{2i\cot(\alpha)}\right)} \\
&\times\Bigg\{\operatorname{erfi}\left(\frac{\sqrt{i/2\cot(\alpha)}}{2} - \frac{i6\pi + iu\operatorname{cosec}(\alpha)}{2\sqrt{i/2\cot(\alpha)}}\right) \\
&- \operatorname{erfi}\left(-\frac{\sqrt{i/2\cot(\alpha)}}{2} - \frac{i6\pi + iu\operatorname{cosec}(\alpha)}{2\sqrt{i/2\cot(\alpha)}}\right)\Bigg\}, \qquad (6)
\end{aligned}
$$

where $\alpha = \beta\pi/2$, *and* $\{\beta \in \mathbb{R}, -1 \le \beta \le 1\}$ *(for* $\beta = 1$, *the proposed approach is summarized in the classical Nuttall window). Proof for (6) is present in Appendix A.*

Traditional windowing approaches demonstrate that decreasing the width of a window function's main lobe typically results in side lobes with greater amplitude, and vice versa. Moreover, to reduce the main lobe width without directly affecting the attenuation of the side lobes, one solution is to increase the number of points in the window. However, this approach can significantly increase complexity and execution time. Depending on the application, such a trade-off becomes critical. As a result, it is often necessary to find a balance when selecting a window function to meet the specific requirements of a given application.

The proposed model overcomes these limitations by enabling a reduction in the main lobe's width without significantly altering the attenuation of the side lobes or increasing the order of the window function. This approach preserves computational complexity and maintains a desirable order, achieved through a mathematical derivation based on the FrFT.

4 Results

In this section, using the approach proposed in Sect. 3, we analyze the performance of the Nuttall windows in the Fourier fractional domain, varying β in the interval [0, 1], and obtaining the following spectral parameters: HMLW, MSLL, and SLFOR.

Looking at Fig. 2 and Table 3, we see the spectral characteristics of each of the

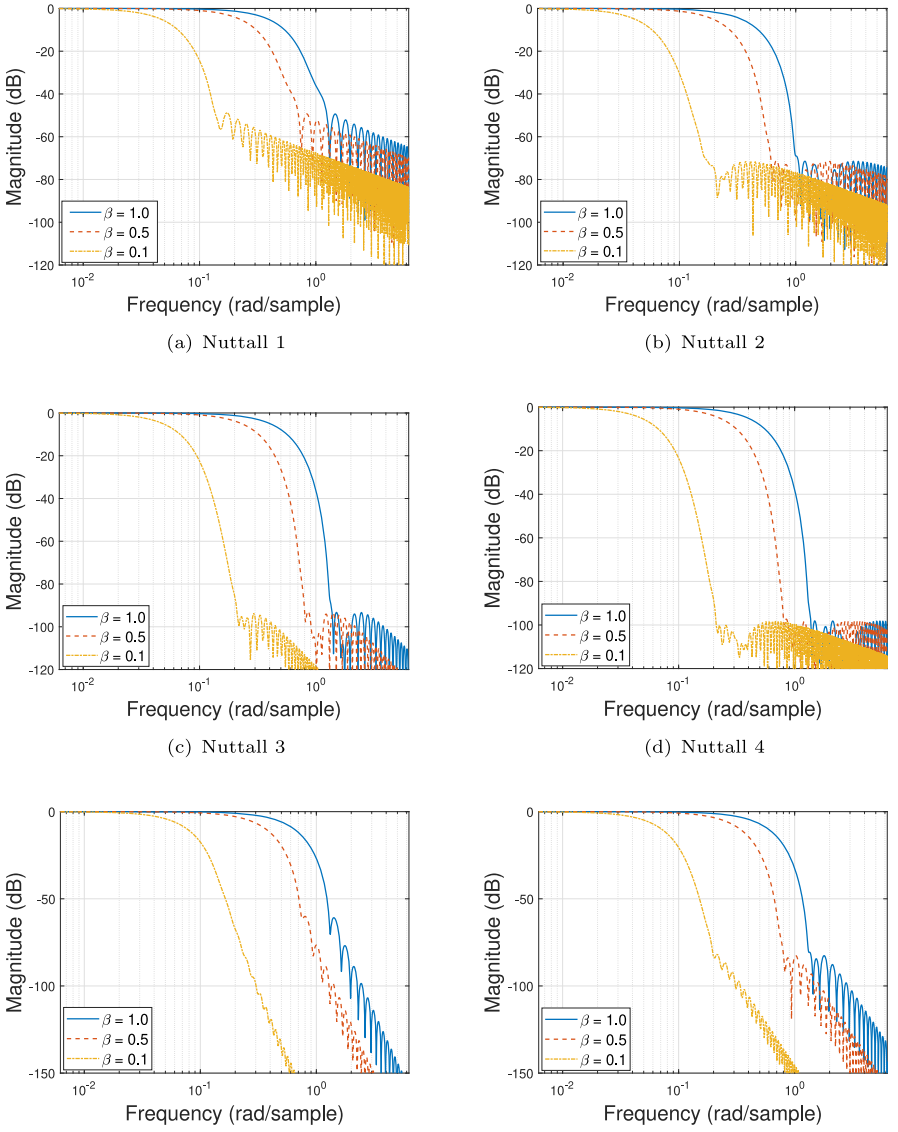

(a) Nuttall 1 (b) Nuttall 2

(c) Nuttall 3 (d) Nuttall 4

(e) Nuttall 5 (f) Nuttall 6

Fig. 2 PSD for Nuttall Windows in the Fourier fractional domain

six Nuttall window functions for $\beta = 0.1; 0.5; 1.0$. We obtained these results using a window function size of 256 points. The HMLW values decrease with β values for all analyzed functions. This is an interesting result because, as mentioned in Sect. 2, windows with large main lobes cause distortions to the signal in the frequency domain, hardening pattern recognition and identification of specific frequency components.

Table 3 Parameters of the Nuttall window functions

β	HMLW (π rad/sample)	MSLL (dB)	SLFOR (dB/oct.)
Nuttall 1			
1.0	1.24	−49.44	7.22
0.5	0.71	−49.46	7.25
0.1	0.14	−48.49	6.35
Nuttall 2			
1.0	1.05	−71.51	4.28
0.5	0.62	−71.61	5.37
0.1	0.19	−71.47	6.16
Nuttall 3			
1.0	1.41	−93.34	15.21
0.5	0.80	−92.91	16.50
0.1	0.21	−93.73	18.66
Nuttall 4			
1.0	1.38	−98.21	0.00
0.5	0.87	−98.26	5.01
0.1	0.21	−98.21	6.37
Nuttall 5			
1.0	1.29	−61.11	44.50
0.5	0.75	−62.74	46.30
0.1	0.31	−104.05	47.70
Nuttall 6			
1.0	1.31	−82.83	27.00
0.5	0.85	−82.62	29.10
0.1	0.20	−82.04	30.57

Analyzing Table 3, we observe that the proposed mathematical approach reduced the HMLW while maintaining the MSLL value for the overall analysis, but significantly decreasing the MSLL for specific windows. For instance, in the Nuttall 5 window with $\beta = 0.1$, the MSLL reached a notable value of -104.05 dB. Regarding the SLFOR parameter, its value increases as the β value decreases. For example, the Nuttall 4 window exhibited an SLFOR increase from 0.00 dB/octave at $\beta = 1.0$ to 6.37 dB/octave at $\beta = 0.1$. It is worth noting that windows with low MSLL and high SLFOR are desirable in spectral analysis, as they help to contain spectral leakage.

We demonstrate the effectiveness of our proposal presented in Sect. 3 through two distinct applications: in Sect. 4.1, a closed-form expression for Nuttall window functions in the FrFT domain is used to identify frequency components in synthetic signals that mimic human respiration. Compared to the traditional approach based on the Fourier transform and traditional window functions, our method significantly reduces distortions such as spectral leakage; in Sect. 4.2, we implemented our approach in a wireless communication scenario, specifically within an F-OFDM system. Our method

significantly improves the filtering performance of F-OFDM, reducing interference between adjacent channels by applying windowing in the FrFT domain.

4.1 Respiratory Rate Monitoring

The respiratory rate is a key indicator of the physiological condition of the human body, and its analysis can provide clues about health issues. Certain devices, such as specific sensors, can effectively monitor the respiratory rate over time [4, 34]. However, the visualization of respiratory frequencies may be affected by potential signal distortions caused by spectral leakage when applying the FT to a time-domain signal [1].

In order to analyze the performance of the proposed approach (6) in a direct application, we applied FrFT to a synthetic signal composed of multiple respiratory frequencies, which could be collected using RF sensors in an enviroment with multiple individuals under healthcare monitoring (e.g., hospital ward), given by:

$$s(t) = \begin{cases} \cos(2\pi 0.1t) & 0s \leq t < 5s, \\ \cos(2\pi 0.5t) & 5s \leq t < 10s, \\ \cos(2\pi 1.0t) & 10s \leq t < 15s, \\ \cos(2\pi 1.5t) & 15s \leq t < 20s. \end{cases} \tag{7}$$

The signal $s(t)$ consists of a set of four sinusoidal waveforms joined in sequence, where each waveform is composed of only one of the four respiratory frequencies 0.1 Hz, 0.5 Hz, 1.0 Hz, 1.5 Hz [4, 14].

Figure 3 shows the spectrograms obtained through the FrFT on $s(t)$ using the Nuttall 1, Nuttall 3, and Nuttall 5 windows, using (6) for $\beta = 1.0$ and $\beta = 0.1$. The colors of the spectrograms in shades of blue and yellow define the magnitude of the signal in dB.

Analyzing the results, it is clear that, for $\beta = 1.0$, the signal with respiratory frequencies is distorted, making it challenging to identify the frequency of interest where the components of each waveform appear, that is, from 0.1 to 1.5 Hz. This distortion occurs due to the wide main lobe present in traditional Nuttall windows. However, we solved this problem reducing the value of β using the approach proposed in (6). For this application, for example, tests were carried out varying β from 1.0 to 0.1. By gradually reducing the β value to the minimum value of 0.1, it was possible to mitigate the distortions caused by spectral leakage. Observing the results for a $\beta = 0.1$ value, it is possible to identify respiratory frequencies in a specific time window. Furthermore, it is worth highlighting that in the signal spectrogram for traditional Nuttall windows (i.e., $\beta = 1.0$) it is possible to identify leakage of signal components to other frequencies, which does not occur in spectrograms with Nuttall windows for $\beta = 0.1$. Therefore, by reducing the value of β, it is possible to improve the performance of the Nuttall window according to the application using the proposed approach, as the MSLL and SLFOR parameters are minimized, reducing spectral leakage to practically zero and improving visualization of the signal and facilitating the identification of the components of the respiratory rate. Therefore, (6) becomes an essential tool in the recognition of patterns in the time-frequency domain, mainly in

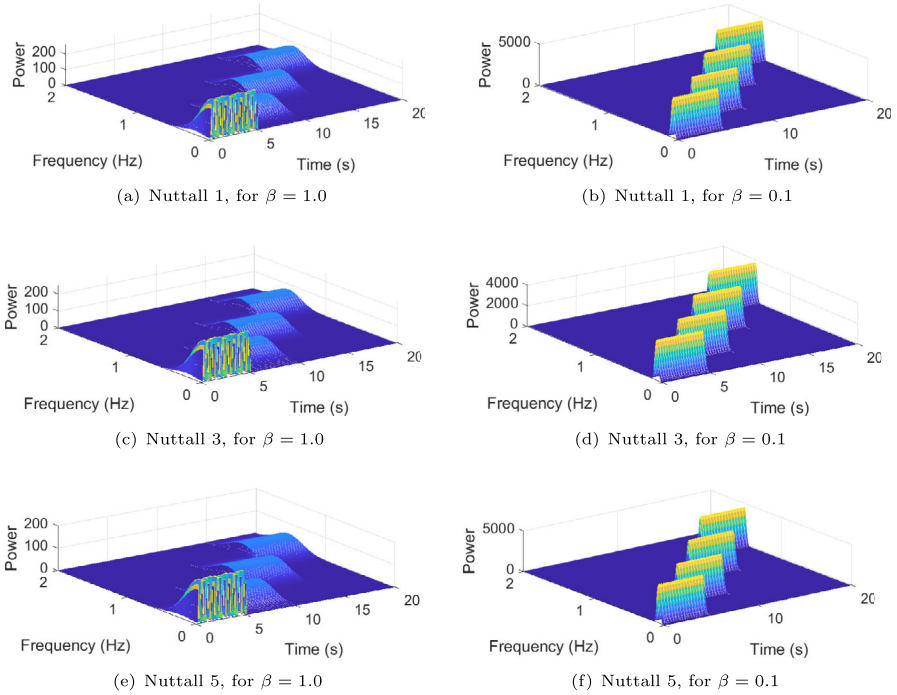

(a) Nuttall 1, for $\beta = 1.0$ (b) Nuttall 1, for $\beta = 0.1$

(c) Nuttall 3, for $\beta = 1.0$ (d) Nuttall 3, for $\beta = 0.1$

(e) Nuttall 5, for $\beta = 1.0$ (f) Nuttall 5, for $\beta = 0.1$

Fig. 3 Spectrograms of the $s(t)$ signal generated using 256-point Nuttall window functions

Table 4 ENBW values

Window Functions	ENBW		
	$\beta = 1.0$	$\beta = 0.5$	$\beta = 0.1$
Nuttall 1	10.0751	5.7519	1.5297
Nuttall 3	10.6859	6.0909	1.5447
Nuttall 5	12.1788	6.9466	1.5909

the identification of possible anomalies that, in many cases, cannot be spotted in the time domain.

We used the Equivalent Noise Bandwith (ENBW) [15] to measure the total leakage of a windowing function. The ENBW measures the ratio between the sum of all the power in a given bandwidth and the main lobe's power. The greater the ENBW value, the more the spectral leakage. Analyzing Table 4, we see that when measuring the ENBW of the Nuttall windows for different values of β, a lower ENBW value is obtained for $\beta = 0.5$ and $\beta = 0.1$, showing that most of the signal power is concentrated in the main lobe. The proposed approach showed a lower ENBW value, easing the identification of respiratory frequencies.

Furthermore, a comparison was made between the proposed approach and the model proposed by [20], where the authors used FrFT with the Generalized Hamming window (more specifically, the Hanning window function). Figure 4 shows a comparison

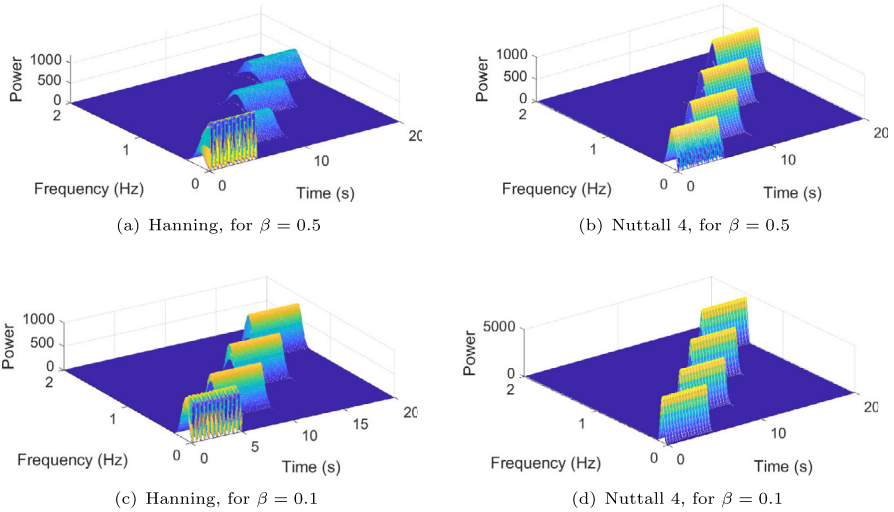

(a) Hanning, for $\beta = 0.5$ (b) Nuttall 4, for $\beta = 0.5$

(c) Hanning, for $\beta = 0.1$ (d) Nuttall 4, for $\beta = 0.1$

Fig. 4 Comparison between spectrograms of the signal $s(t)$ from the Hanning and Nuttall 4 window functions using a size of 256 points

between spectrograms obtained through FrFT for both windows, that is, with Nuttall 4 (our proposal) and Hanning (proposed by [20]). Analyzing the results, it is clear that, for the exact value of β, the model proposed by [20] presents a signal with respiratory frequencies with an inevitable distortion, even with the reduction of the β parameter, making it challenging to identify the frequency of interest where the components of each waveform appear, that is, from 0.1 to 1.5 Hz. This does not occur in the proposed model using the Nuttall window, where it is possible to identify respiratory frequencies in a specific time window for $\beta = 0.5$ and $\beta = 0.1$.

4.2 Wireless Communication

mMTC is a key use case of 5G networks, enabling a large number of devices to seamlessly intercommunicate within the 5G infrastructure. By enabling many connected sensors, mMTC facilitates smart agriculture and Industry 4.0 [24]. To achieve this, the network must efficiently use the radio spectrum to support many sensors connected to the network [6]. It is known that Orthogonal Frequency-Division Multiplexing (OFDM) is the waveform used in 5G networks. However, one of its disadvantages is the high OOBE, which reduces spectral efficiency, demanding guard bands to mitigate interference between subbands. This issue can be addressed by applying windowing/filtering to the OFDM waveform (F-OFDM).

Signal transmission in an F-OFDM system differs from the OFDM system by the introduction of a low-pass filter, named the windowed-sinc filter [17, 38]:

$$h(l) = \frac{p(l) \cdot w(l)}{\sum_i p(i) \cdot w(i)}, \tag{8}$$

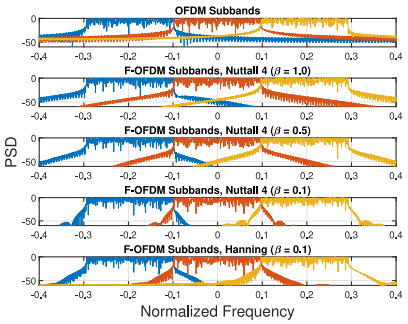

(a) Number of filter coefficients: 64 points

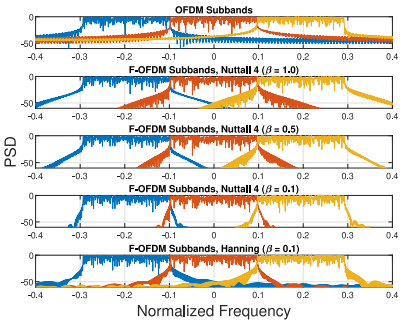

(b) Number of filter coefficients: 128 points

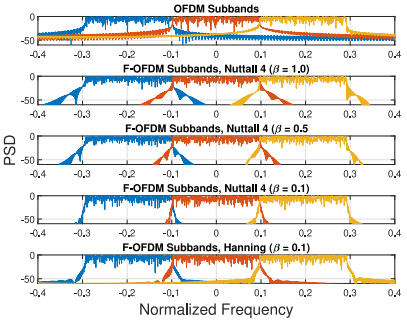

(c) Number of filter coefficients: 256 points

Fig. 5 PSD for an F-OFDM signal using the proposed approach with variation in the number of coefficients of the windowed-sinc filter, and the number of points

and, $p(l) = \text{sinc}\left(\Delta f\ (K + 2R)\ \frac{l}{N_{ifft}}\right)$, for $-L/2 \leq l \leq L/2$, where L is the filter order, $p(l)$ is the sinc function, $w(l)$ is the window function, Δf denotes the interval between subcarriers, K is the number of subcarriers, R denotes bandwidth excess, and N_{ifft} is the IFFT order.

Therefore, the F-OFDM signal ($\tilde{s}(t)$) is obtained by applying the normalized filter $h(l)$ to the OFDM signal in each subband, as follows:

$$\tilde{s}(t) = \sum_{k=0}^{K-1} a_{n,k}\upsilon\left(t - nT_f\right) e^{j2\pi k\Delta f\left(t-nT_f\right)} \otimes h\left(t - nT_f\right), \tag{9}$$

where $\otimes$ represents the convolution operation, k is the subcarrier index, $\upsilon(t)$ denotes the pulse shape, $a_{n,k}$ is the complex data of the n-th OFDM symbol carried by the k-th subcarrier.

The Nuttall 4 window is used in this communication scenario based on the F-OFDM technology, as it is the window with the best performance in terms of MSLL. Figure 5 presents PSD for the F-OFDM subband (with bandwidth = 20 MHz and 64-QAM modulation), and Fig. 6 presents BER using the closed-form expression (6), for

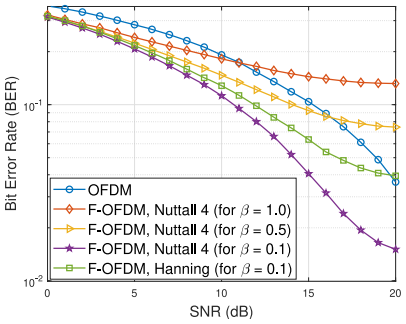

(a) Number of filter coefficients: 64 points

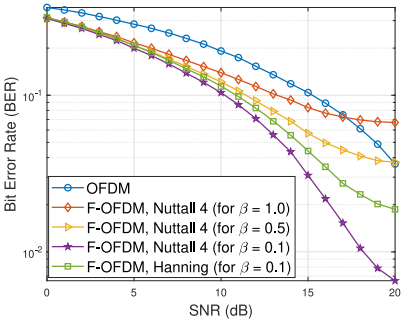

(b) Number of filter coefficients: 128 points

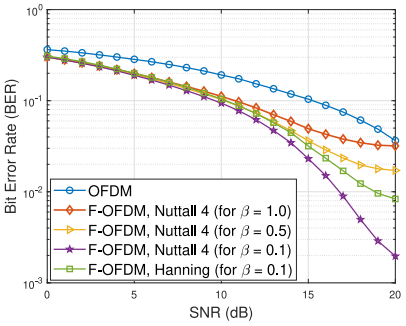

(c) Number of filter coefficients: 256 points

Fig. 6 BER for an OFDM and F-OFDM signal using the proposed approach and Hamming window function with variation in the number of coefficients of the windowed-sinc filter, and the number of points

$\beta = 1.0$, 0.5 and 0.1.

Analyzing Fig. 5, we observe that applying filtering to subbands using the proposed approach significantly reduces OOBE by varying the value of β and/or increasing the filter coefficients. This reduction in OOBE is achieved by decreasing the power of the side lobes in adjacent channels or, rather, by increasing the attenuation rate of the side lobes in the subbands. This improvement is due to the reduction in the ENBW value for the Nuttall 4 when we have $\beta < 1$.

For example, using Nuttall 4 for $\beta = 1$, we have an average ENBW value of 10.4480. In contrast, for $\beta = 0.1$, the ENBW value drops to 1.5196, significantly reducing the spectral leakage outside the band of interest. It is worth mentioning that, when using the proposed approach in composing the windowed-sinc filter, it is possible to reduce the OOBE even using a reduced number of points, e.g., compare in Fig. 5 results for $\beta = 1.0$ and 256 points with those obtained using only 64 or 128 points and $\beta = 0.1$. Despite the reduced number of points, the latter results present better performance than the former one. Furthermore, it is worth noting that when compared with the model proposed in [20] (Hanning with FrFT), our approach proved to be superior even for $\beta = 1$ for both proposals.

Furthermore, by analyzing Fig. 6, it can be seen that the reduction in OOBE positively impacts the BER of the F-OFDM system when there is a variation in the Signal-to-Noise Ratio (SNR). It can be seen that the lower the value of β, the better the system performance in terms of BER, and this occurs due to the reduction of interference between subbands of adjacent channels, meaning that the transmitted bits do not suffer distortions, facilitating demodulation in the OFDM receiver for 5G and B5G networks.

5 Conclusion and Future Work

The traditional Nuttall window function (1) has the advantage of having four coefficients (Table 1), allowing the adjustment of its spectral parameters: HMLW, MSLL, and SLFOR. However, even after changing its coefficients, this window function presents a wide HMLW in the frequency domain, which is not ideal and can be a problem depending on the chosen application. For this reason, this work proposes a mathematical model combining the Nuttall window function with the FrFT (6), since combining these two approaches can mitigate this issue by means of the adjustable β parameter. This parameter reduced the HMLW for all six window functions presented in this work. In addition, in some cases, it was possible to increase the performance of specific windows, in terms of MSLL and SLFOR, with emphasis on the following windows: Nuttal 5, reducing the MSLL from -61.11 to -104.05 dB; and Nuttall 4, raising the SLFOR from 0.00 to 6.37 dB/octave. The performance of Nuttall windows using (6) was evaluated using signals in the human respiratory frequencies ($s(t)$). The signal spectrograms with Nuttall windows for $\beta = 0.1$ reduced signal distortions compared to those with Nuttall windows for $\beta = 1.0$. Therefore, this enables the identification of the exact frequencies where the signal components are located. Furthermore, the performance of Nuttall windows using (6) was evaluated in the F-OFDM system to solve one of the major issues of this technology, OOBE. The proposed window has the advantage of having a higher attenuation rate of the side lobes. Consequently, the F-OFDM signal using the proposed approach concentrates more power in the main lobe.

For future work, initially, we intend to use an optimization algorithm to find the optimal values for the coefficients and the β parameter of the proposed approach. Subsequently, we will use the proposed model to analyze and recognize patterns and anomalies in heartbeat signals via EEG sensors.

Appendix A Proof of Proposition 1 in Section 3

Nuttall windows are fixed window functions whose main characteristic is an excellent attenuation of the side lobes due to the values of their coefficients (a_n, for $n = 0, 1, 2, ..., N-1$) that multiply each term in the sum-cosine expression. However, since they have a low amplitude in the side lobes, this reflects a high main lobe width [25, 28]. To mitigate this problem, a mathematical approach is proposed in which the behavior of Nuttall windows in the FrFT domain is analyzed.

Proof Rewriting (1) in Euler's formula, we have:

$$w(t) = a_0 + a_1 \frac{\mathrm{e}^{i2\pi t} + \mathrm{e}^{-i2\pi t}}{2} + a_2 \frac{\mathrm{e}^{i4\pi t} + \mathrm{e}^{-i4\pi t}}{2} + a_3 \frac{\mathrm{e}^{i6\pi t} + \mathrm{e}^{-i6\pi t}}{2}, \ |t| \leq \frac{1}{2}. \tag{A1}$$

Applying the FrFT given by (4) in (A1), we have:

$$\begin{aligned} W_\alpha(u) = {} & a_0 \sqrt{\frac{1 - i\cot(\alpha)}{2\pi}} e^{i\frac{u^2}{2}\cot(\alpha)} \\ & \times \int_{-1/2}^{1/2} \mathrm{e}^{\left[i\frac{t^2}{2}\cot(\alpha) - iut\,\mathrm{cosec}(\alpha)\right]} dt \\ & + \frac{a_1}{2} \sqrt{\frac{1 - i\cot(\alpha)}{2\pi}} e^{i\frac{u^2}{2}\cot(\alpha)} \\ & \times \int_{-1/2}^{1/2} e^{i2\pi t} \mathrm{e}^{\left[i\frac{t^2}{2}\cot(\alpha) - iut\,\mathrm{cosec}(\alpha)\right]} dt \\ & + \frac{a_1}{2} \sqrt{\frac{1 - i\cot(\alpha)}{2\pi}} e^{i\frac{u^2}{2}\cot(\alpha)} \\ & \times \int_{-1/2}^{1/2} e^{-i2\pi t} \mathrm{e}^{\left[i\frac{t^2}{2}\cot(\alpha) - iut\,\mathrm{cosec}(\alpha)\right]} dt \\ & + \frac{a_2}{2} \sqrt{\frac{1 - i\cot(\alpha)}{2\pi}} e^{i\frac{u^2}{2}\cot(\alpha)} \\ & \times \int_{-1/2}^{1/2} e^{i4\pi t} \mathrm{e}^{\left[i\frac{t^2}{2}\cot(\alpha) - iut\,\mathrm{cosec}(\alpha)\right]} dt \\ & + \frac{a_2}{2} \sqrt{\frac{1 - i\cot(\alpha)}{2\pi}} e^{i\frac{u^2}{2}\cot(\alpha)} \\ & \times \int_{-1/2}^{1/2} e^{-i4\pi t} \mathrm{e}^{\left[i\frac{t^2}{2}\cot(\alpha) - iut\,\mathrm{cosec}(\alpha)\right]} dt \\ & + \frac{a_3}{2} \sqrt{\frac{1 - i\cot(\alpha)}{2\pi}} e^{i\frac{u^2}{2}\cot(\alpha)} \\ & \times \int_{-1/2}^{1/2} e^{i6\pi t} \mathrm{e}^{\left[i\frac{t^2}{2}\cot(\alpha) - iut\,\mathrm{cosec}(\alpha)\right]} dt \\ & + \frac{a_3}{2} \sqrt{\frac{1 - i\cot(\alpha)}{2\pi}} e^{i\frac{u^2}{2}\cot(\alpha)} \\ & \times \int_{-1/2}^{1/2} e^{-i6\pi t} \mathrm{e}^{\left[i\frac{t^2}{2}\cot(\alpha) - iut\,\mathrm{cosec}(\alpha)\right]} dt. \end{aligned} \tag{A2}$$

The Eq. (A2) is rewritten as follows:

$$W_\alpha(u) = W_a^0 + W_\alpha^1 + W_\alpha^2 + W_\alpha^3 + W_\alpha^4 + W_\alpha^5 + W_\alpha^6. \tag{A3}$$

Solving each term separately in (A3), we have:

$$\begin{aligned}
W_\alpha^0(u) &= a_0\sqrt{\frac{1-i\cot(\alpha)}{2\pi}}e^{i\frac{u^2}{2}\cot(\alpha)} \\
&\quad\times\int_{-1/2}^{1/2} \mathrm{e}^{\left[i\frac{t^2}{2}\cot(\alpha)-iut\operatorname{cosec}(\alpha)\right]}dt \\
&= \frac{a_0}{2}\sqrt{\frac{1-i\cot(\alpha)}{i\cot(\alpha)}}e^{\frac{u^2}{2}\left(i\cot(\alpha)+\frac{\operatorname{cosec}(\alpha)^2}{i\cot(\alpha)}\right)} \\
&\quad\times\left\{\operatorname{erfi}\left(\frac{\sqrt{i/2\cot(\alpha)}}{2}-\frac{iu\operatorname{cosec}(\alpha)}{2\sqrt{i/2\cot(\alpha)}}\right)\right. \\
&\quad\left.-\operatorname{erfi}\left(-\frac{\sqrt{i/2\cot(\alpha)}}{2}-\frac{iu\operatorname{cosec}(\alpha)}{2\sqrt{i/2\cot(\alpha)}}\right)\right\}.
\end{aligned} \tag{A4}$$

$$\begin{aligned}
W_\alpha^1(u) &= \frac{a_1}{2}\sqrt{\frac{1-i\cot(\alpha)}{2\pi}}e^{i\frac{u^2}{2}\cot(\alpha)} \\
&\quad\times\int_{-1/2}^{1/2} e^{i2\pi t}\mathrm{e}^{\left[i\frac{t^2}{2}\cot(\alpha)-iut\operatorname{cosec}(\alpha)\right]}dt \\
&= \frac{a_1}{4}\sqrt{\frac{1-i\cot(\alpha)}{i\cot(\alpha)}}e^{\left(i\frac{u^2}{2}\cot(\alpha)-\frac{(i2\pi-iu\operatorname{cosec}(\alpha))^2}{2i\cot(\alpha)}\right)} \\
&\quad\times\left\{\operatorname{erfi}\left(\frac{\sqrt{i/2\cot(\alpha)}}{2}+\frac{i2\pi-iu\operatorname{cosec}(\alpha)}{2\sqrt{i/2\cot(\alpha)}}\right)\right. \\
&\quad\left.-\operatorname{erfi}\left(-\frac{\sqrt{i/2\cot(\alpha)}}{2}+\frac{i2\pi-iu\operatorname{cosec}(\alpha)}{2\sqrt{i/2\cot(\alpha)}}\right)\right\}.
\end{aligned} \tag{A5}$$

$$\begin{aligned}
W_\alpha^2(u) &= \frac{a_1}{2}\sqrt{\frac{1-i\cot(\alpha)}{2\pi}}e^{i\frac{u^2}{2}\cot(\alpha)} \\
&\quad\times\int_{-1/2}^{1/2} e^{-i2\pi t}\mathrm{e}^{\left[i\frac{t^2}{2}\cot(\alpha)-iut\operatorname{cosec}(\alpha)\right]}dt \\
&= \frac{a_1}{4}\sqrt{\frac{1-i\cot(\alpha)}{i\cot(\alpha)}}e^{\left(i\frac{u^2}{2}\cot(\alpha)-\frac{(-i2\pi-iu\operatorname{cosec}(\alpha))^2}{2i\cot(\alpha)}\right)} \\
&\quad\times\left\{\operatorname{erfi}\left(\frac{\sqrt{i/2\cot(\alpha)}}{2}-\frac{i2\pi+iu\operatorname{cosec}(\alpha)}{2\sqrt{i/2\cot(\alpha)}}\right)\right. \\
&\quad\left.-\operatorname{erfi}\left(-\frac{\sqrt{i/2\cot(\alpha)}}{2}-\frac{i2\pi+iu\operatorname{cosec}(\alpha)}{2\sqrt{i/2\cot(\alpha)}}\right)\right\}.
\end{aligned} \tag{A6}$$

$$\begin{aligned}
W_\alpha^3(u) &= \frac{a_2}{2}\sqrt{\frac{1-i\cot(\alpha)}{2\pi}}e^{i\frac{u^2}{2}\cot(\alpha)} \\
&\quad\times\int_{-1/2}^{1/2} e^{i4\pi t}\mathrm{e}^{\left[i\frac{t^2}{2}\cot(\alpha)-iut\operatorname{cosec}(\alpha)\right]}dt
\end{aligned}$$

$$= \frac{a_2}{4}\sqrt{\frac{1-i\cot(\alpha)}{i\cot(\alpha)}}e^{\left(i\frac{u^2}{2}\cot(\alpha)-\frac{(i4\pi-iu\operatorname{cosec}(\alpha))^2}{2i\cot(\alpha)}\right)} \times\left\{\operatorname{erfi}\left(\frac{\sqrt{i/2\cot(\alpha)}}{2}+\frac{i4\pi-iu\operatorname{cosec}(\alpha)}{2\sqrt{i/2\cot(\alpha)}}\right)-\operatorname{erfi}\left(-\frac{\sqrt{i/2\cot(\alpha)}}{2}+\frac{i4\pi-iu\operatorname{cosec}(\alpha)}{2\sqrt{i/2\cot(\alpha)}}\right)l\right\}. \tag{A7}$$

$$W_\alpha^4(u) = \frac{a_2}{2}\sqrt{\frac{1-i\cot(\alpha)}{2\pi}}e^{i\frac{u^2}{2}\cot(\alpha)} \times\int_{-1/2}^{1/2} e^{-i4\pi t}\mathrm{e}^{\left[i\frac{t^2}{2}\cot(\alpha)-iut\operatorname{cosec}(\alpha)\right]}dt$$

$$= \frac{a_2}{4}\sqrt{\frac{1-i\cot(\alpha)}{i\cot(\alpha)}}e^{\left(i\frac{u^2}{2}\cot(\alpha)-\frac{(-i4\pi-iu\operatorname{cosec}(\alpha))^2}{2i\cot(\alpha)}\right)} \times\left\{\operatorname{erfi}\left(\frac{\sqrt{i/2\cot(\alpha)}}{2}-\frac{i4\pi+iu\operatorname{cosec}(\alpha)}{2\sqrt{i/2\cot(\alpha)}}\right)-\operatorname{erfi}\left(-\frac{\sqrt{i/2\cot(\alpha)}}{2}-\frac{i4\pi+iu\operatorname{cosec}(\alpha)}{2\sqrt{i/2\cot(\alpha)}}\right)\right\}. \tag{A8}$$

$$W_\alpha^5(u) = \frac{a_3}{2}\sqrt{\frac{1-i\cot(\alpha)}{2\pi}}e^{i\frac{u^2}{2}\cot(\alpha)} \times\int_{-1/2}^{1/2} e^{i6\pi t}\mathrm{e}^{\left[i\frac{t^2}{2}\cot(\alpha)-iut\operatorname{cosec}(\alpha)\right]}dt$$

$$= \frac{a_3}{4}\sqrt{\frac{1-i\cot(\alpha)}{i\cot(\alpha)}}e^{\left(i\frac{u^2}{2}\cot(\alpha)-\frac{(i6\pi-iu\operatorname{cosec}(\alpha))^2}{2i\cot(\alpha)}\right)} \times\left\{\operatorname{erfi}\left(\frac{\sqrt{i/2\cot(\alpha)}}{2}+\frac{i6\pi-iu\operatorname{cosec}(\alpha)}{2\sqrt{i/2\cot(\alpha)}}\right)-\operatorname{erfi}\left(-\frac{\sqrt{i/2\cot(\alpha)}}{2}+\frac{i6\pi-iu\operatorname{cosec}(\alpha)}{2\sqrt{i/2\cot(\alpha)}}\right)\right\}. \tag{A9}$$

$$W_\alpha^6(u) = \frac{a_3}{2}\sqrt{\frac{1-i\cot(\alpha)}{2\pi}}e^{i\frac{u^2}{2}\cot(\alpha)} \times\int_{-1/2}^{1/2} e^{-i6\pi t}\mathrm{e}^{\left[i\frac{t^2}{2}\cot(\alpha)-iut\operatorname{cosec}(\alpha)\right]}dt$$

$$= \frac{a_3}{4}\sqrt{\frac{1-i\cot(\alpha)}{i\cot(\alpha)}}e^{\left(i\frac{u^2}{2}\cot(\alpha)-\frac{(-i6\pi-iu\operatorname{cosec}(\alpha))^2}{2i\cot(\alpha)}\right)} \times\left\{\operatorname{erfi}\left(\frac{\sqrt{i/2\cot(\alpha)}}{2}-\frac{i6\pi+iu\operatorname{cosec}(\alpha)}{2\sqrt{i/2\cot(\alpha)}}\right)-\operatorname{erfi}\left(-\frac{\sqrt{i/2\cot(\alpha)}}{2}-\frac{i6\pi+iu\operatorname{cosec}(\alpha)}{2\sqrt{i/2\cot(\alpha)}}\right)\right\}. \tag{A10}$$

Replacing (A4)–(A10) in (A3) the proposed mathematical model is obtained. □

Acknowledgements The authors would like to thank Coordenação de Aperfeiçoamento de Pessoal de Nível Superior (CAPES), Fundação de Amparo à Pesquisa no Estado de Goiás (FAPEG), and Centro de

Excelência em Redes Inteligentes sem Fio (CERISE) for the financial support in the development of this research.

Author Contributions Not applicable.

Funding This study was partially funded by the Coordenação de Aperfeiçoamento de Pessoal de Nível Superior (CAPES) - Brazil - Finance Code 001, and by the Fundação de Amparo à Pesquisa do Estado de Goiás (FAPEG) through the Centro de Excelência em Redes Inteligentes sem Fio (CERISE).

Data Availability Not applicable.

Code Availability Not applicable.

Declarations

Conflict of interest The authors declare that they have no known competing financial interests or personal relationships that could have appeared to influence the work reported in this paper.

Ethics approval and consent to participate Not applicable.

Consent for publication Not applicable.

Materials availability Not applicable.

References

1. S. Abbas, S. Ojo, A. Al Hejaili, G.A. Sampedro, A. Almadhor, M.M. Zaidi, N. Kryvinska, Artificial intelligence framework for heart disease classification from audio signals. Sci. Rep. **14**, 3123 (2024)
2. A. Abdulwahhab Mohammed, A.H. Abdulwahhab, Analysis of potential 5g transmission methods concerning bit error rate. AEU-Int. J. Electron. C. **184**, 155407 (2024). https://doi.org/10.1016/j.aeue.2024.155407
3. G. An, M. Akiba, K. Omodaka, T. Nakazawa, H. Yokota, Hierarchical deep learning models using transfer learning for disease detection and classification based on small number of medical images. Sci. Rep. **11**(1), 4250 (2021)
4. A.M. Ashleibta, Q.H. Abbasi, S.A. Shah, M.A. Khalid, N.A. AbuAli, M.A. Imran, Non-invasive rf sensing for detecting breathing abnormalities using software defined radios. IEEE Sens. J. **21**(4), 5111–5118 (2021). https://doi.org/10.1109/JSEN.2020.3035960
5. V. Catană, I.M. Flondor, M. Scumpu, α-windowed fourier transform (α-wft). J. Pseudo-Differ. Oper. Appl. (2024). https://doi.org/10.1007/s11868-024-00644-9
6. I.B.F. de Almeida, L.L. Mendes, J.J.P.C. Rodrigues, M.A.A. da Cruz, 5g waveforms for iot applications. IEEE Commun. Surv. Tutor. **21**(3), 2554–2567 (2019). https://doi.org/10.1109/COMST.2019.2910817
7. N. Dissanayake, C.U.S. Edussooriya, C. Wijenayake, A. Madanayake, Multibeam wideband transmit beamforming using 2d sparse fir trapezoidal filters. J. Low Power Electron. Appl. **14**(2), 26 (2024). https://doi.org/10.3390/jlpea14020026
8. J. Gautam, A. Kumar, R. Saxena, Windows: a tool in signal processing. IETE Tech. Rev. **12**(3), 217–226 (1995)
9. N. Goel, J. Kaur, Analysis of pc6 window function using fractional Fourier transform. Opto-Electron. Eng. **45**(6), 1707451–1707459 (2018). https://doi.org/10.12086/oee.2018.170745
10. N. Goel, J. Singh, Analysis of Kaiser and Gaussian window functions in the fractional Fourier transform domain and its application. Iran. J. Sci. Technol. Trans. Electr. Eng. **43**(2), 181–188 (2019)
11. P. Guan, D. Wu, T. Tian, J. Zhou, X. Zhang, L. Gu, A. Benjebbour, M. Iwabuchi, Y. Kishiyama, 5g field trials: Ofdm-based waveforms and mixed numerologies. IEEE J. Sel. Areas Commun. **35**(6), 1234–1243 (2017)
12. A. Hammoodi, L. Audah, M. Taher, Green coexistence for 5g waveform candidates: a review. IEEE Access **7**, 10103–10126 (2019)

13. F. Harris, The examination of cell on the use of windows for harmonic analysis with the discrete Fourier transform. Proc. IEEE **66**(1), 51–83 (1978)
14. D. Jarchi, D. Salvi, L. Tarassenko, D.A. Clifton, Validation of instantaneous respiratory rate using reflectance ppg from different body positions. Sensors (2018). https://doi.org/10.3390/s18113705
15. H. Jokinen, J. Ollila, O. Aumala, On windowing effects in estimating averaged periodograms of noisy signals. Measurement **28**(3), 197–207 (2000)
16. S. Kavusi, H. Kakavand, A. Gamal, On incremental sigma-delta modulation with optimal filtering. IEEE Trans. Circuits Syst. I Regul. Pap. **53**(5), 1004–1015 (2006). https://doi.org/10.1109/TCSI.2006.870218
17. T. Kebede, Y. Wondie, J. Steinbrunn, H.B. Kassa, K.T. Kornegay, Multi-carrier waveforms and multiple access strategies in wireless networks: performance, applications, and challenges. IEEE Access **10**, 21120–21140 (2022). https://doi.org/10.1109/ACCESS.2022.3151360
18. J. Koester, J.S. Chen, Conforming window functions for meshfree methods. Comput. Methods Appl. Mech. Eng. **347**(2019), 588–621 (2019)
19. E. Koç, T. Alikaşifoğlu, A.C. Aras, A. Koç, Trainable fractional Fourier transform. IEEE Signal Process. Lett. **31**, 751–755 (2024). https://doi.org/10.1109/LSP.2024.3372779
20. S. Kumar, K. Singh, R. Saxena, Analysis of Dirichlet and generalized "hamming" window functions in the fractional Fourier transform domains. Signal Process. **91**(2011), 600–606 (2011)
21. J. Li, Z. Dong, L. Luo, S. Duan, L. Wang, A novel versatile window function for memristor model with application in spiking neural network. Neurocomputing **405**, 239–246 (2020)
22. M. Liu, Y. Chen, Z. Zhang, S. Deng, Classification of power quality disturbance using segmented and modified s-transform and dcnn-msvm hybrid model. IEEE Access **11**, 890–899 (2023). https://doi.org/10.1109/ACCESS.2022.3233767
23. P.V. Muralidhar, S. Nayak, T. Sahu, Implementation of fractional Fourier transform in digital filter design. J. Commun. **15**(3), 289–302 (2020). https://doi.org/10.12086/oee.2018.170745
24. W. Nakimuli, J. Garcia-Reinoso, J.E. Sierra-Garcia, P. Serrano, I.Q. Fernández, Deployment and evaluation of an industry 4.0 use case over 5g. IEEE Commun. Mag. **59**(7), 14–20 (2021). https://doi.org/10.1109/MCOM.001.2001104
25. A. Nuttall, Some windows with very good sidelobe behavior. IEEE Trans. Acoust. Speech Signal Process. **29**(1), 217–226 (1981)
26. H. Ozaktas, M. Kutay, D. Mendlovic, Introduction to the fractional Fourier transform and its applications. Adv. Imaging Electron Phys. **106**, 239–291 (1999)
27. R.K. Pooja Mohindru, S.S. Bhatia, Spectral analysis of generalized triangular and welch window functions using fractional Fourier transform. Automatika **57**(1), 221–229 (2016)
28. K. Prabhu, *Window Functions and Their Applications in Signal Processing* (CRC Press, Taylor & Francis Group, Boca Raton, 2013)
29. C.M. Sandino, J.Y. Cheng, F. Chen, M. Mardani, J.M. Pauly, S.S. Vasanawala, Compressed sensing: from research to clinical practice with deep neural networks: shortening scan times for magnetic resonance imaging. IEEE Signal Process. Mag. **37**(1), 117–127 (2020)
30. K.K. Sharma, S.D. Joshi, Signal separation using linear canonical and fractional Fourier transforms. Opt. Commun. **265**(2), 454–460 (2006). https://doi.org/10.1016/j.optcom.2006.03.062
31. V. Stanković, Adjustable high resolution window function. Electron. Lett. **54**(13), 827–829 (2018)
32. M.F. Tang, B. Su, Joint window and filter optimization for new waveforms in multicarrier systems. EURASIP J. Adv. Signal Process. **63**(2018), 1–20 (2018)
33. H.H. Xie, Q. Chen, Development of distributed low voltage distribution remote monitoring system. J. Phys. Conf. Ser. **1550**(5), 052011 (2020). https://doi.org/10.1088/1742-6596/1550/5/052011
34. Y. Yan, S.B. Samdin, K.N. Minhad, Window-based time-frequency methods for analyzing epileptic eeg signals, in *2022 IEEE-EMBS Conference on Biomedical Engineering and Sciences (IECBES)*, pp. 292–297, (2022)
35. M. Yang, Y. Chen, L. Du, Interference analysis and filter parameters optimization for uplink asynchronous f-ofdm systems. IEEE Access **7**, 48356–48370 (2019). https://doi.org/10.1109/ACCESS.2019.2910592
36. Y. Yang, Q. Wu, S.T. Jhang, 2d linear canonical transforms on lp and applications. Fractal Fract. (2023). https://doi.org/10.3390/fractalfract7020100
37. S. Zhang, J. Liu, T.K. Rodrigues, N. Kato, Deep learning techniques for advancing 6g communications in the physical layer. IEEE Wirel. Commun. **28**(5), 141–147 (2021)

38. X. Zhang, M. Jia, L. Chen, J. Ma, J. Qiu, Filtered-ofdm: enabler for flexible waveform in the 5th generation cellular networks, in *2015 IEEE Global Communications Conference (GLOBECOM)*, pp. 1–6 (2015)
39. Z. Zhao, G. Li, Synchrosqueezing-based short-time fractional Fourier transform. IEEE Trans. Signal Process. **71**, 279–294 (2023). https://doi.org/10.1109/TSP.2023.3244097